# On the crystallization of solid formers during liquefaction of gases

Marco Campestrini, Salem Hoceini, Paolo Stringari, Nicolò Baiguini

# On the crystallization of solid formers during liquefaction of gases

Marco Campestrini*, Salem Hoceini, Paolo Stringari, Nicolò Baiguini

*Mines Paris, PSL University, Centre for Thermodynamics of Processes (CTP), 77300 Fontainebleau, France*

## Abstract

Besides well-known technologies for the liquefaction of air components ($N_2$, Ar, and $O_2$) that of $CH_4$, $H_2$, and $CO_2$ has recently caught attention for the energy transition and climate change targets. Gases undergoing cryogenic processes (cooling, liquefaction, cryo-compression) can contain a certain number of impurities, thus one challenge encountered in liquefaction is the solidification of heavy compounds present in the feed. In dealing with the crystallization risk of solid formers during liquefaction, attention is nowadays addressed to their solubility limits in the liquefied gas at the lowest temperature of the process, because solubility is known to decrease for decreasing temperatures. These limits are then used for tailoring the purification steps upstream the liquefaction train or modifying the operative conditions of the plant to avoid solid formation.

In this work, the modeling and the analysis of the available data of several binary mixtures (like $H_2$+$N_2$, $N_2$+$CO_2$, $CH_4$+$CO_2$, and $CO_2$+$nC_{10}H_{22}$) allow drawing insights about the thermodynamic behavior of such mixtures at low temperatures, showing that the lowest solubility limits are not always encountered at the lowest temperature, and this may have an impact on the design of industrial liquefaction processes. According to the liquefaction pressure, the first risk of solidification of the heaviest component could indeed be related to the deposition from the vapor phase rather than the solidification from the liquid phase.

As a matter of fact, solubility limits of a solid former could be lower in a warmer gaseous/supercritical solvent than in a colder liquid solvent, thus solid formation could occur at temperatures that are up to tens of degrees higher than the final liquefaction temperature.

Consequently, front-end purification units reducing the content of solid formers in the feed below their solubility limits in the liquefied gas could not be sufficient to completely avoid the risk of crystallization as temperature decreases.

Keywords: Liquefaction of gases, Crystallization risk, Deposition, Solidification, Hydrogen, Methane, Carbon dioxide

# 1 Introduction

Liquefaction of gases is a key process for several applications, like aerospace, petrochemistry, health, electronics, metallurgy, and energy transportation and storage [1-7].

A better understanding of the cryogenic phase equilibrium behavior of binary systems composed by fluids of quite different relative volatility (as hydrogen + nitrogen, methane + benzene, and nitrogen + carbon dioxide) is mandatory to assure correct process design and safe operating conditions of processing and liquefaction of the most volatile fluid in the mixture.

Faced with the problem of solidification of impurities in cryogenic processes dealing with the liquefaction of light gases (like hydrogen, methane, air components, and carbon dioxide), it has become imperative to find ways to master the solubility limits of solid formers in light component-rich mixtures (where solid former means an impurity that can solidify because its triple-point temperature is higher than the temperatures encountered by the stream in the liquefaction process).

In dealing with the crystallization risk of solid formers during the liquefaction of (i) natural gas (i.e. n-alkanes up to $nC_9H_{20}$ and $nC_{10}H_{22}$, cyclo-alkanes, branched-alkanes, aromatics, carbon dioxide, hydrogen sulfide), (ii) biomethane (mainly carbon dioxide and hydrogen sulfide), (iii) hydrogen (air components, methane, carbon dioxide, carbon monoxide according to the $H_2$ production technology), (iv) main air components (mainly carbon dioxide and nitrous oxide), and (v) carbon dioxide (depending of the $CO_2$ emitting process), attention is usually almost entirely addressed to the solubility limits of the cited impurities in the liquefied gas (hydrogen, methane, nitrogen, oxygen, and carbon dioxide).

When experimental values (from the literature) or calculated values (from reliable thermodynamic models) dealing with the composition of a solid former "*i*" in the liquid phase (almost pure light-component) at Solid-Liquid Equilibrium (SLE) are available, a simple comparison between these phase equilibrium values and the compositions of "*i*" in the gaseous stream feeding the liquefaction plant points out (i) the need (or not) of a purification step for reducing the composition of "*i*" below

its solubility limit and (ii) the interest of setting operative conditions different from those affected by SLE conditions throughout the process.

More generally, N potential solid formers can be identified in the multicomponent mixture of vector of global composition $\bar{z}_1$ feeding the liquefaction plant by comparing their triple-point or melting temperature and the final liquefaction temperature ($T_3$) of the process, Fig. 1.

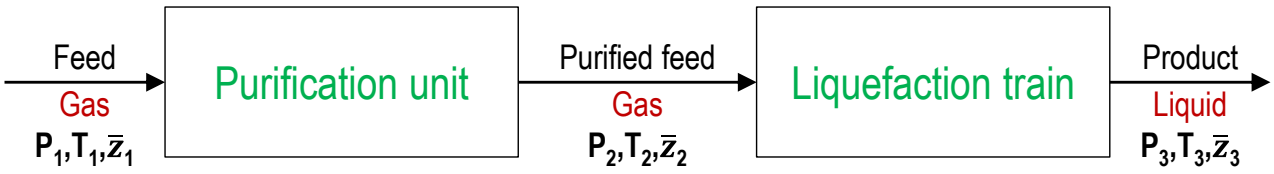


**Fig. 1.** Schematic representation of purification unit and liquefaction train.
$P_1$, $T_1$, $\bar{z}_1$: pressure, temperature, and vector of global molar composition of the feed; $P_2$, $T_2$, $\bar{z}_2$: pressure, temperature, and vector of global molar composition of the purified feed; $P_3$, $T_3$, $\bar{z}_3$: pressure, temperature, and vector of global molar composition of liquefied gas. If crystallization does not occur, $\bar{z}_2 = \bar{z}_3$.

Considering that the solubility $x$ of a solid former in a liquid solvent is known to decrease for decreasing temperatures (exponentially, according to the classical approach, Eq. (1)), the front-end purification unit upstream the liquefaction train is tailored in order to decrease the global molar composition of each solid former $i$ in the feed $z_{1,i}$ down a value $z_{2,i}$ that is lower than its solubility limit at solid-liquid equilibrium in the liquefied gas ($x_{3,i}$) at the final liquefaction temperature ($T_3$), namely $z_{1,i}$ ($P_1$, $T_1$) > $z_{2,i}$ ($P_2$, $T_2$) = $z_{3,i}$ ($P_3$, $T_3$) < $x_{3,i}$ ($P_3$, $T_3$).

For sake of completeness, the classical approach for calculating the solubility of solid component in the liquid phase according to its activity coefficient ($\gamma$), latent heat of melting ($\Delta H_m$) and triple-point temperature $T_T$, latent heat of each $i^{th}$ solid-solid transition ($\Delta H_{SS,i}$) and corresponding transition temperature ($T_{SS,i}$), is reported in Eq. (1) of this work, [8].

$$x\gamma = \exp\left[\frac{\Delta H_m}{RT_T} - \frac{\Delta H_m}{RT} + \sum_{i=1}^{N}\left(\frac{\Delta H_{SS,i}}{RT_{SS,i}} - \frac{\Delta H_{SS,i}}{RT}\right)\right] \quad (1)$$

The objective of this work is highlighting that the solid phase can originate, from a thermodynamic point of view, from either a liquid or a vapor media during the liquefaction of a gas according to the pressure of the liquefaction train.

## 2 The phase diagram of light component + solid former binary mixtures

Considering literature works dealing with the global phase equilibrium behavior (fluid + solid phases) of binary mixtures composed by components of quite different volatility, as those resumed or given in Refs. [9-16], there is solid evidence to suggest that the qualitative pressure-temperature phase equilibrium behavior of a generic Light Component (LC) + heavy component or Solid Former (SF) mixture in proximity of the saturation line of LC can be resumed as in Fig. 2(A). To demonstrate, Fig. 2(A) (and the following) has been drawn by considering the global phase equilibrium behavior of more than 50 binary mixtures involving in particularly hydrogen, helium, methane, nitrogen, argon, oxygen, and carbon dioxide as LC.

The qualitative phase equilibrium behavior in Fig. 2(A) presents the Vapor-Liquid Equilibrium (VLE) of LC (blue line), a portion of the critical locus of the mixture (V = L, red dashed line), and a portion of the Solid-Liquid-Vapor Equilibrium (SLVE) branch of the mixture. With respect to this latter, the corresponding black continuous line becomes dashed because different thermodynamic conditions can be encountered at temperatures higher than the critical-point temperature of LC, as shown in the following (the same applies also for the critical locus of the mixture).

In Fig. 2(A), the VLE line of LC extends from the low-pressure region up to its critical point (the blue point); the mixture critical locus originates from the critical point of LC and moves towards higher temperatures and pressures; finally, each pressure-temperature couple lying on the SLVE line refers to an equilibrium between a solid phase (that can be approximated to some extent as made by pure SF) and two LC-rich fluid phases (liquid and vapor).

In the low-pressure region (not shown in Fig. 2(A)), the VLE curve ends at the triple point of LC, whereas the SLVE curve joins a quadruple point accounting for the equilibrium between two solid phases (solid LC and solid SF), a liquid phase, and a vapor phase.

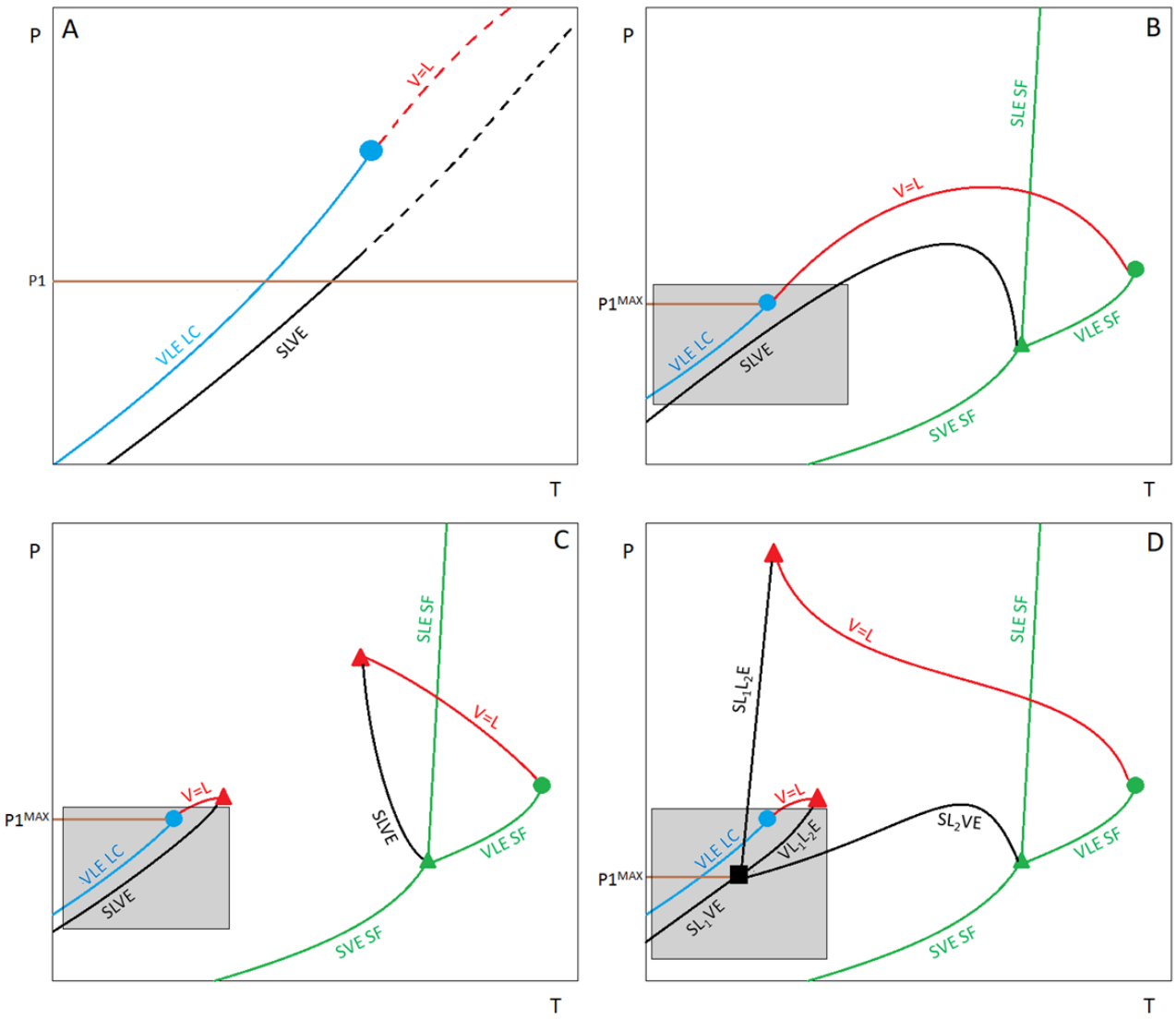


**Fig. 2.** Phase equilibrium behavior of a generic Light Component (LC) + Solid Former (SF) mixture in proximity of the saturation line of LC (A), and at temperatures higher than the triple point temperature of LC while having a fluid-fluid phase equilibrium behavior of type I (B), IIIc (C), and IIIa (D) according to the van Konynenburg and Scott's classification.
— : VLE of pure LC; ● : critical point of LC; — : VLE, SLE, and SVE of pure SF; ● : critical point of SF; ▲ : triple point of SF; ▲ : Upper Critical EndPoint (UCEP); —, - - : triple-point curve of the mixture (SLVE, $SL_1L_2E$, $SL_1VE$, $SL_2VE$); —, - - : critical locus of the mixture; ■ : quadruple point ($SL_1L_2VE$); P1 : system pressure; $P1^{MAX}$ : maximum value for P1. Subscripts: 1 : related to LC; 2 : related to SF.

The behavior of the SLVE in the high-pressure region has not been intentionally drawn seeing that three main possibilities can occur according to the collected literature works:

- Fig. 2(B): the SLVE and critical loci join the triple and critical points of the heavy component in the mixture (SF), respectively. Examples of systems whose thermodynamic behavior is qualitatively resumed as in Fig. 2(B) are $CH_4$ + $CO_2$/$nC_4H_{10}$/$nC_5H_{12}$, $N_2$ + $O_2$/Ar/Kr/$CH_4$, $O_2$ + Ar/Kr/Xe/$CH_4$, Ar + Kr/Xe/$CH_4$, Kr + Xe, and $CO_2$ + $nC_4H_{10}$/$nC_5H_{12}$/$nC_6H_{14}$. Mixtures whose thermodynamic equilibrium behavior is qualitatively illustrated in Fig. 2(B) are of type I according to the van Konynenburg and Scott's classification [17] and of type D according to that of Kohn and Luks [14].
- Fig. 2(C): the critical locus originating at the critical point of LC and the SLVE branch join together a singular point, called Upper Critical EndPoint (UCEP), where SF is at equilibrium with a LC-rich critical phase. Examples of systems whose thermodynamic behavior is qualitatively resumed as in Fig. 2(C) are $CH_4$+$C_6H_6$/$nC_8H_{18}$/$nC_{10}H_{22}$, $N_2$ + Xe/Ne/$CO_2$/$N_2O$, $O_2$ + Ne/He/$CO_2$/$N_2O$, Ar + Ne/$CO_2$, He + Ne, $CO_2$ + $nC_{22}H_{46}$, and $H_2$ + $N_2$/$O_2$/Ar/$CH_4$. Mixtures whose thermodynamic equilibrium behavior is qualitatively illustrated in Fig. 2(C) are of type IIIc according to the van Konynenburg and Scott's classification [17] and of type A according to that of Kohn and Luks [14].
- Fig. 2(D): the SLVE ($SL_1VE$) line joins a quadruple point accounting for the Solid-$Liquid_1$-$Liquid_2$-Vapor Equilibrium ($SL_1L_2VE$), where subscripts 1 and 2 refer to LC-rich and SF-rich phase, respectively. Three other 3-phase equilibrium curves originate from the quadruple point: the Solid-$Liquid_2$-Vapor Equilibrium ($SL_2VE$) branch joining the triple point of SF, the Vapor-$Liquid_1$-$Liquid_2$ Equilibrium ($VL_1L_2E$) branch joining an UCEP together with the critical line leaving the critical point of LC, and the Solid-$Liquid_1$-$Liquid_2$ Equilibrium ($SL_1L_2E$) branch which extends in the high-pressure region. Examples of systems whose thermodynamic behavior is qualitatively resumed as in Fig. 2(D) are $CH_4$ + $H_2S$/$C_7H_8$/$nC_7H_{16}$, $O_2$ + $nC_3$/$C_3H_6$, $N_2$ + $C_2H_6$/$C_2H_4$/$nC_3H_8$/$C_6H_6$, and $CO_2$ + n-alkane from $nC_{14}H_{30}$ up to $nC_{21}H_{44}$. Mixtures whose thermodynamic equilibrium behavior is qualitatively

illustrated in Fig. 2(D)) are of type IIIa according to the van Konynenburg and Scott's classification [17] and of type B according to that of Kohn and Luks [14].

In Fig. 2(B-D), the saturation (VLE), melting (SLE), and sublimation (SVE) loci of SF (heaviest component in the mixture) are highlighted in green, whereas the critical loci (V=L) are highlighted in red.

The high-temperature region of these possible configurations is no more addressed in this work because the main objective is discussing a direct consequence of the reciprocal position of the VLE curve of LC and the SLVE curve illustrated in Fig. 2(A) and in the gray boxes of Fig. 2(B-D), at least up to a certain maximum pressure ($P1^{MAX}$).

The pressure P1 indicated in Fig. 2(A) is intended to increase up to a maximum value ($P1^{MAX}$ in Fig. 2(B-D)): this maximum pressure roughly corresponds to the critical-point pressure of LC for mixtures behaving like the ones in Fig. 2(B,C), whereas the pressure at the quadruple point accounting for the $SL_1L_2VE$ is usually the boundary for those mixtures whose phase diagram is qualitatively illustrated in Fig. 2(D).

The following analysis is valid for any pressure P1 (highlighted by the horizontal brown line in Fig. 2(A)) up to $P1^{MAX}$.

## 3 The temperature-composition phase diagram of LC + SF binary mixtures

Fig. 3 portrays the temperature-composition phase diagram of a generic LC + SF mixture in proximity of the saturation temperature of LC at the pressure P1 (lower than the critical-point pressure of LC as in Fig. 2(A)).

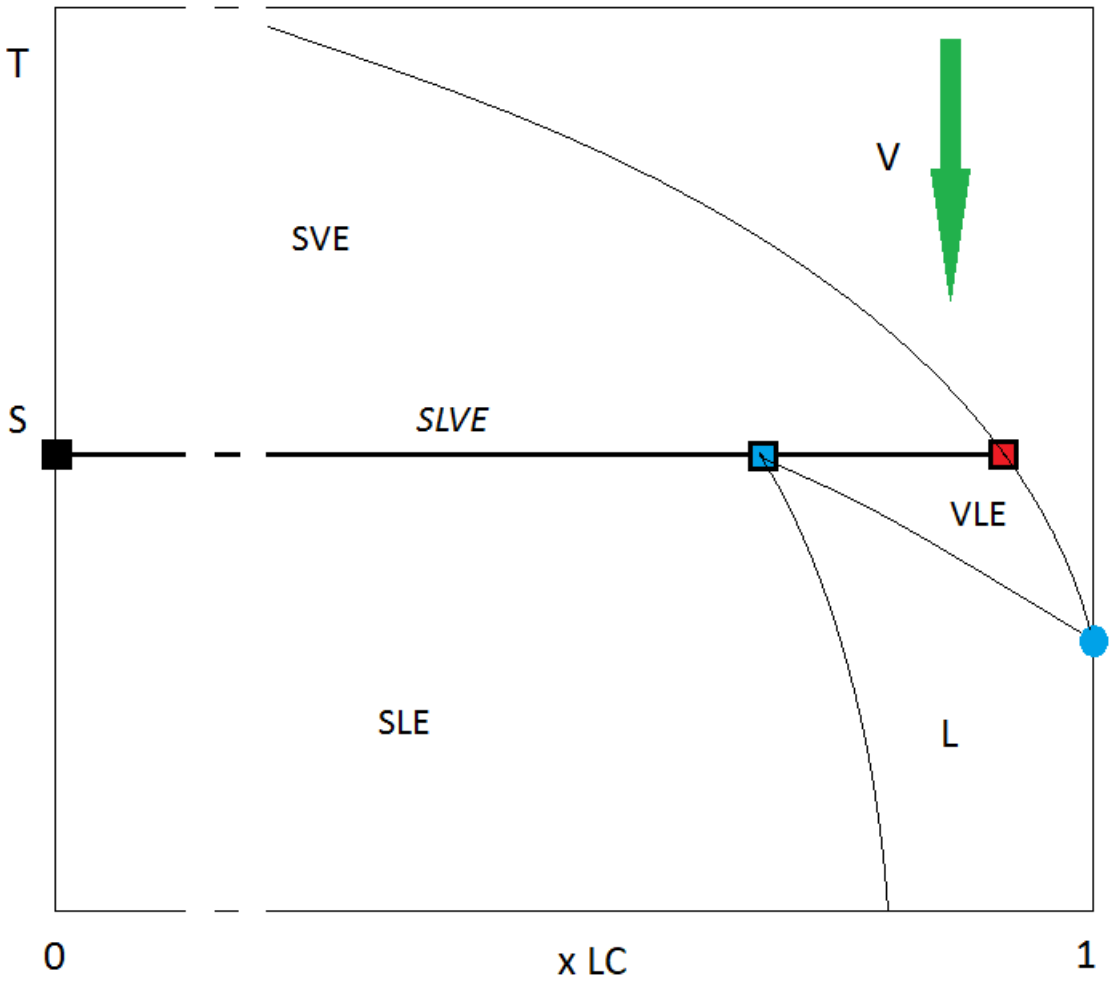


**Fig. 3.** Temperature-composition phase diagram at pressure P1 of a generic LC + SF mixture in proximity of the saturation temperature of LC.
L : liquid phase: V : vapor phase; S ; solid phase; — : equilibrium composition of the vapor phase at SVE, of the liquid phase at SLE, and of the vapor and liquid phases at VLE; ▬ : SLVE temperature; ■ : mole fraction of LC in the vapor phase at SLVE; ■ : mole fraction of LC in the liquid phase at SLVE; ■ : mole fraction of LC in the solid phase (assumed pure SF) at SLVE; ● : saturation temperature of LC at P1.

The horizontal line in Fig. 3 has been drawn at the SLVE temperature: the solid phase (supposed made of pure solid former) is at equilibrium with a liquid phase and a vapor phase richer in LC. The compositions of the liquid and vapor phases are pointed out by the blue and red square, respectively.

The SLVE occurs at a temperature higher than the VLE temperature of pure LC (the blue point of Fig. 3) seeing that in Fig. 2(A) the SLVE curve is placed to the right of the saturation line of LC. As a consequence, the LC-content in the vapor phase at SLVE temperature is higher than the one in the liquid phase at the same temperature.

In addition to that, the forms of the Solid-Vapor Equilibrium (SVE), SLE, and VLE are such that a LC-rich liquid phase is stable also at temperatures higher than the saturation temperature of LC at the pressure P1. In fact, the liquidus branch related to the SLE extends up to the blue square placed at the SLVE temperature.

When a LC-rich mixture is cooled in a liquefaction process (roughly represented by the downward green arrow of Fig. 3) two cases (A and B) can take place according to the composition of the mixture. It has to be clarified here that the liquefaction process discussed in this section does not include the pressure-reduction step commonly involved in industrial liquefaction plant (which involves for instance a Joule-Thomson valve) to produced liquefied gas at pressures suitable for its transport and storage (typically atmospheric pressure), rather it ends with the liquefied gas leaving for instance the last cryogenic heat exchanger at given design pressure. Case A and case B are illustrated in Fig. 4 and Fig. 5, respectively.

In Figs. 4-5, the liquefaction process (schematically represented by the green vertical line) is supposed cooling the LC-rich mixture, leaving the purification unit and feeding the liquefaction train with a LC-content indicated by the green point, from the temperature $T_{IN}$ down to the temperature of the liquefied gas $T_{OUT}$, whose LC-content is indicated by the black point. In both Figs. 4 and 5, the LC-content related to the solubility limit of SF in the liquid phase at $T_{OUT}$ is indicated by the red circle.

By taking into account only the reciprocal position of green (LC-content in the feed) and red (LC-content in the liquid phase corresponding to the solubility limit of SF in LC at SLE) points in Figs. 4-5, it can be stated that a suitable purification unit is used in the liquefaction plant, seeing that the LC-content in the gas stream undergoing liquefaction is higher than the LC-content related to the solubility of SF at the SLE at $T_{OUT}$. Consequently, it can be concluded that the liquefaction of the LC-rich gaseous mixture leaving the purification unit does not present any crystallization risk down to $T_{OUT}$.

The cooling process in Fig. 4 will indeed decrease the temperature of the gaseous stream till obtaining a saturated vapor phase by reaching the dew-point temperature of the mixture at the given pressure P1 (the upper green square in Fig. 4); a vapor and a liquid phase will then coexist at VLE down to a saturated liquid phase at the bubble-point temperature of the mixture at the given pressure P1 (the lower green square in Fig. 4). The further cooling of the mixture will decrease the temperature of the liquefied gas down to $T_{OUT}$.

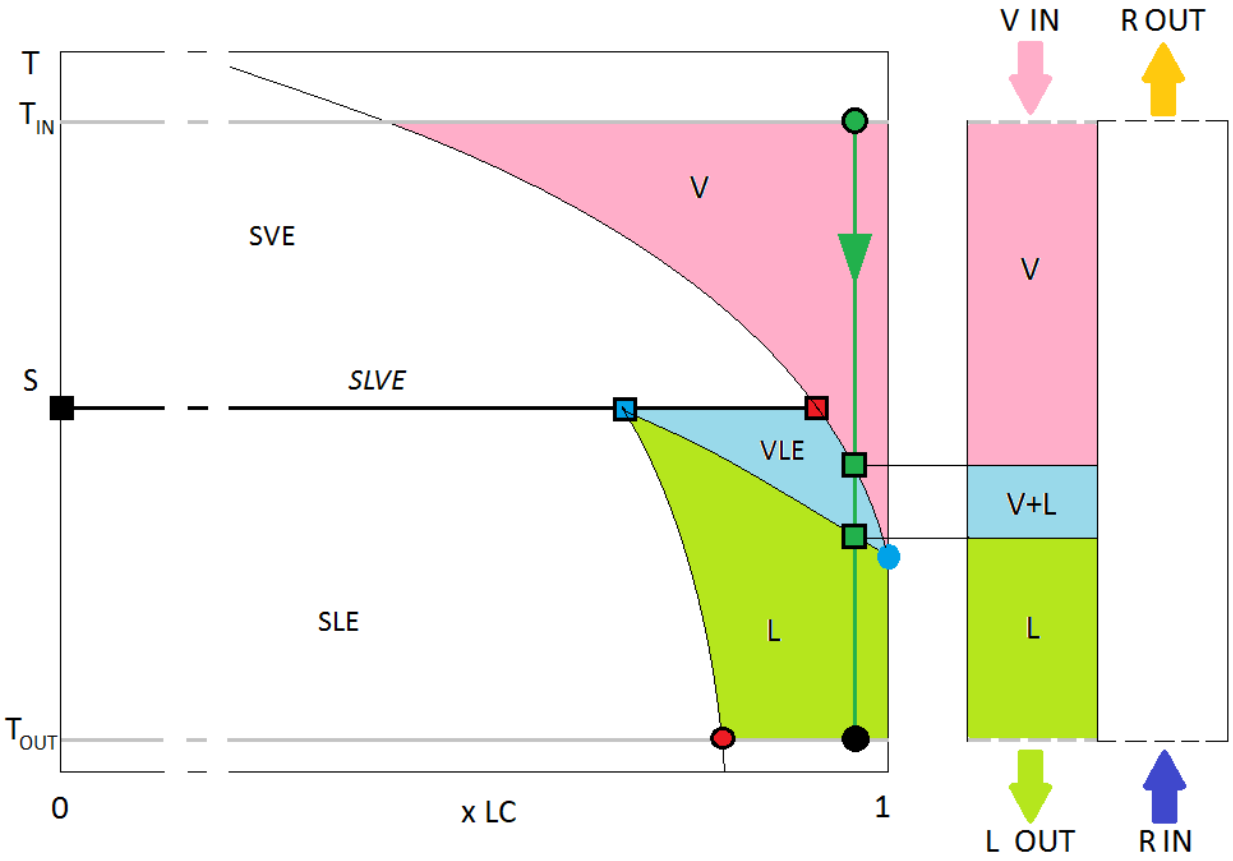


**Fig. 4.** Thermodynamics of the liquefaction process in the temperature-composition phase diagram of a generic LC + SF mixture in proximity of the saturation temperature of LC. Case A: absence of solid deposition.
L : liquid phase: V : vapor phase; S ; solid phase; R : refrigerant; IN : input; OUT : output; — : equilibrium compositions at SVE, SLE, or VLE; ▬ : SLVE temperature; ■ : mole fraction of LC in the vapor phase at SLVE; ■ : mole fraction of LC in the liquid phase at SLVE; ■ : mole fraction of LC in the solid phase (assumed pure SF) at SLVE; ■ : mole fraction of LC in the saturated vapor phase (upper) and in the saturated liquid phase (lower) at VLE; ● : saturation temperature of LC; ● : mole fraction of LC at the temperature of the output liquefied gas; ● : mole fraction of LC at the temperature of the input gas; ● : mole fraction of LC in the liquid phase at SLE at $T_{OUT}$.

The thermodynamic behavior of the liquefaction process is roughly represented in a hypothetical section of the heat exchanger needed for the liquefaction, drawn on the right side of Figs. 4 and 5. G IN and L OUT stand for the gas input and liquefied gas output, respectively. The streams of the input and output refrigerant mixture are instead indicated as R IN and R OUT. The two streams (gas to be liquefied and refrigerant) have been supposed in countercurrent.

The channel of the heat exchanger where the LC-rich mixture is flowing is full of gas till the first drop of liquid phase is formed once the dew-point temperature is reached (upper green square in Fig. 4). A vapor and a liquid phase will coexist at VLE in a certain section of the channel between the two green squares, then only the liquid phase will flow in the whole sections of the channel as the temperature decreases below the bubble-point temperature of the mixture at P1 down to $T_{OUT}$.

To the contrary, in Fig. 5 the cooling process will decrease the temperature of the LC-rich gas mixture till the solid appearance temperature where a saturated vapor phase is at equilibrium with a solid phase (pure SF). This vapor phase is indicated by the upper green square of Fig. 5.

As a consequence, a solid phase deposits according to the phase equilibrium behavior of the binary mixture (kinetic aspects have to be taken into account for evaluating if solid crystals can nucleate and grow).

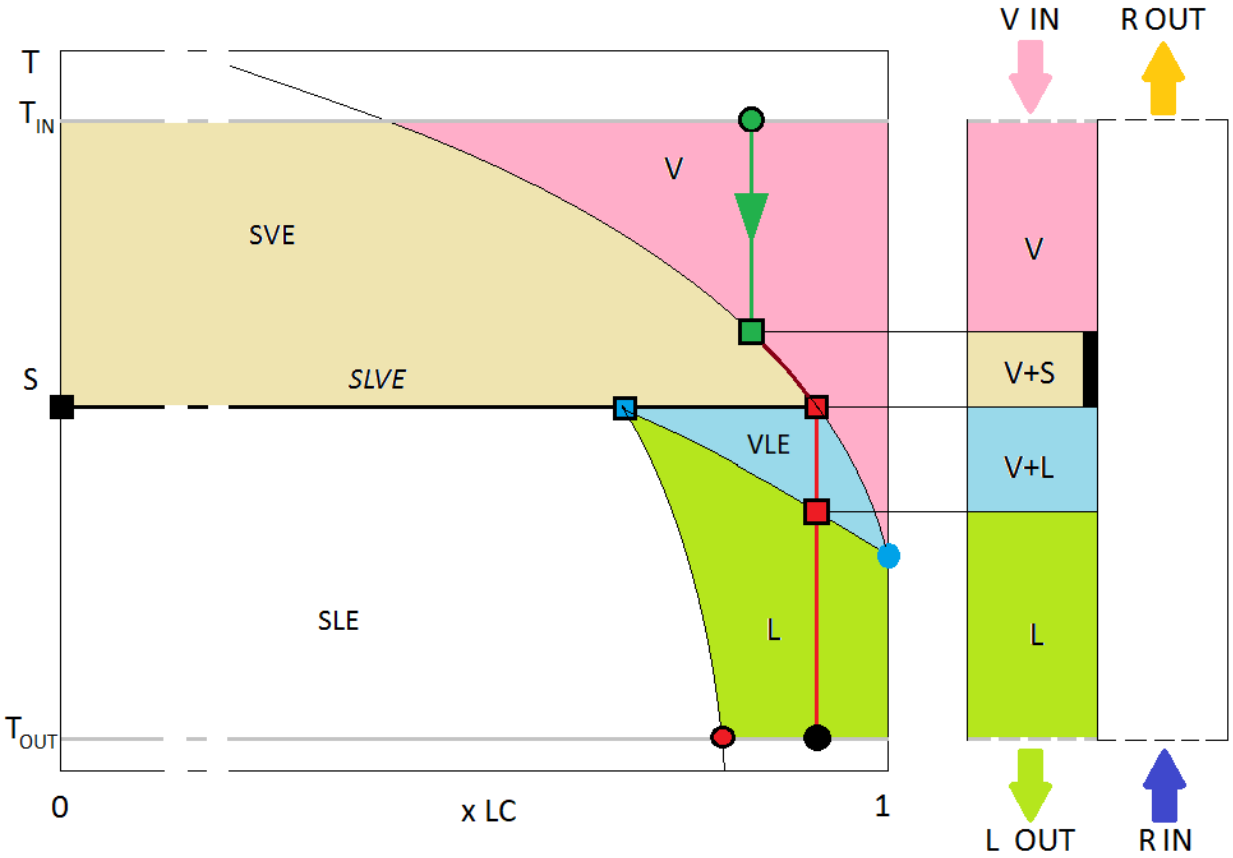


**Fig. 5.** Thermodynamics of the liquefaction process in the temperature-composition phase diagram of a generic LC + SF mixture in proximity of the saturation temperature of LC. Case B: solid deposition.
L : liquid phase: V : vapor phase; S ; solid phase; R : refrigerant; IN : input; OUT : output; — : equilibrium compositions at SVE, SLE, or VLE; ▬ : SLVE temperature; ■ (upper point): mole fraction of LC in the vapor phase at SLVE; ■ : mole fraction of LC in the liquid phase at SLVE; ■ : mole fraction of LC in the solid phase (assumed pure SF) at SLVE; ■ (lower point): mole fraction of LC in the saturated liquid phase at VLE; ■ : mole fraction of LC in the saturated vapor phase at SVE; ● : saturation temperature of LC; ● : mole fraction of LC at the temperature of the output liquefied gas; ● : mole fraction of LC at the temperature of the input gas; ● : mole fraction of LC in the liquid phase at SLE at $T_{OUT}$.

The solid deposit has been pointed out by a black block in Fig. 5. The vapor phase and the pure solid former in the solid phase will then coexist at equilibrium down to the SLVE temperature, at which the first drop of liquid occurs.

According to the temperature diagram in Fig. 5, the solid phase should not deposit in the channels of the heat exchanger for temperatures lower than the SLVE temperature seeing that the LC-rich mixture (whose composition is now equal to the one of the saturated vapor phase at SLVE) enters in a VLE condition. Under hypotheses that the vapor and liquid phases will flow simultaneously in the channels of the heat exchanger, the VLE will occur between the SLVE temperature and the bubble-

point temperature (lower red square in Fig. 5). When the temperature reaches the liquidus boundary of the VLE, the LC-rich mixture has been totally liquefied and the temperature can be decreased down to the required $T_{OUT}$.

To sum up and from the low-temperature/cryogenic thermodynamic behavior of several binary mixtures composed by a light component and a solid former, the liquefaction of a gaseous mixture with a LC-content higher than the composition of the vapor phase at the SLVE temperature of Fig. 4 will occur without solidification of the solid former. If the liquefaction involves a LC-rich gas having a LC-content higher than the value related to the solubility limit of the solid former at $T_{OUT}$ but lower than the LC-composition in the vapor phase at SLVE will entail the deposition of a solid phase in the heat exchanger. In addition to that, this solid phase will not be at equilibrium with a liquid phase but with a vapor phase.

Similar analysis could be also carried out at higher pressures ($P > P1^{MAX}$) for systems having a fluid-phase diagram of type IIIc according to the classification of van Konynenburg and Scott, Fig. 2(C): the presence of the VLE "triangle" in the temperature-composition phase diagram in Fig. 3 entails a S-loop for the transition between SVE and SLE at pressure higher than the UCEP pressure of the system (the one close to the critical point of LC), see Fig. 6. Despite authors does not find lot of direct evidence in the available literature (one example is given for the methane + p-xylene system in Ref. [18]), such a behavior is confirmed by the analysis of existing SLE and SVE data, and by modeling results concerning plenty of the binary mixtures of the IIIc type involved in this work.

This behavior is related to the rapid change in density of the LC-rich solvent passing from a vapor phase at SVE to a liquid phase at SLE in proximity of the critical-point region of LC; in this temperature region, the combined effect of temperature (solubility decreases for decreasing temperatures) and of density (solubility increases for increasing densities) results in such a S-loop shape.

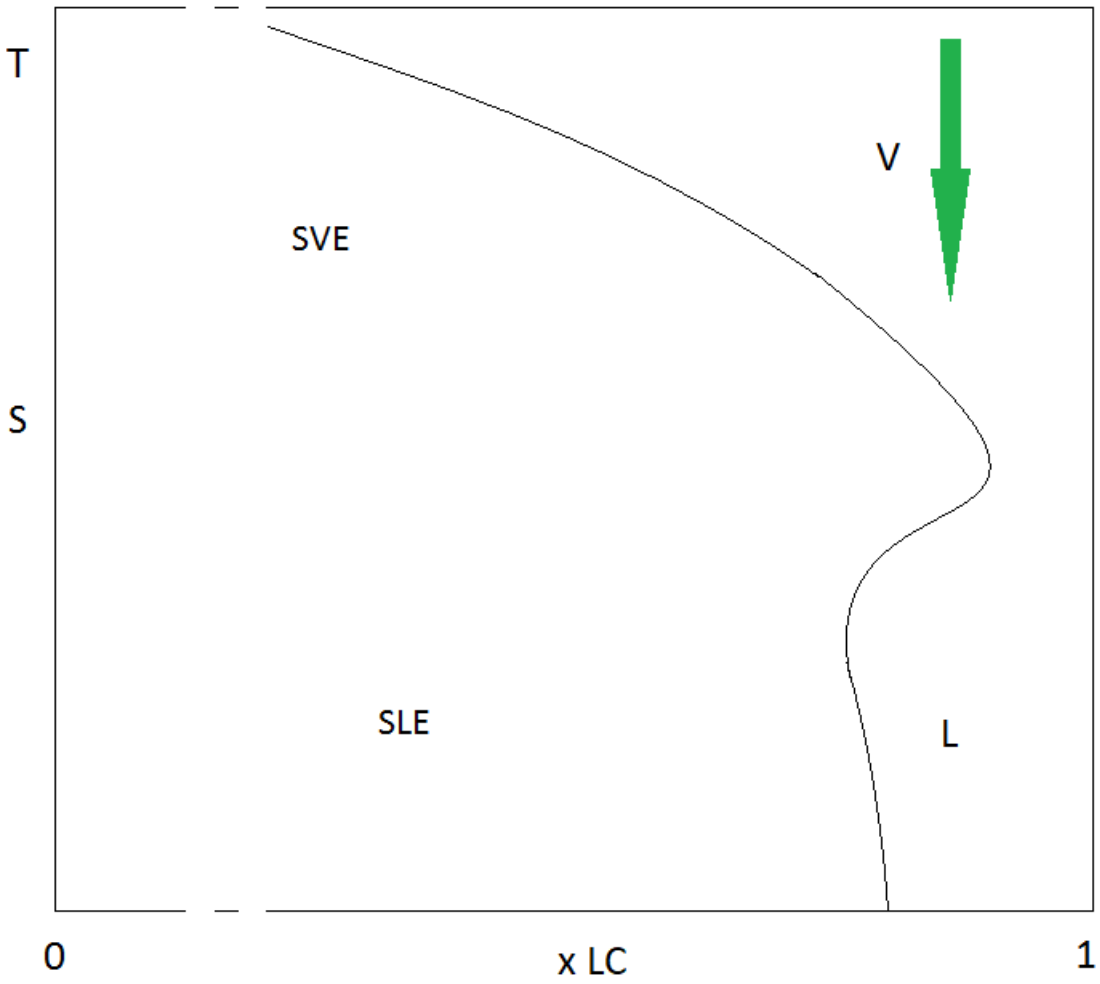


**Fig. 6.** Temperature-composition phase diagram at pressure higher than $P1^{MAX}$ of a generic LC + SF mixture in proximity of the critical temperature of LC for systems having global phase diagram of type IIIc.
L : liquid phase: V : vapor phase; S ; solid phase; — : equilibrium composition of the vapor phase at SVE and of the liquid phase at SLE.

## 4 Analysis of the $H_2$ + $N_2$, $N_2$ + $CO_2$, and $CH_4$ + $CO_2$ systems

To illustrate the conclusions drawn in previous section by keeping into account qualitative behaviors of a certain number of binary mixtures, modeling results are presented in this section for the hydrogen + nitrogen, nitrogen + carbon dioxide, and methane + carbon dioxide systems.

For the modeling work, the Peng-Robinson Equation of State (PR EoS, [19]) has been used for representing both vapor and liquid phases and coupled with classical approach, Eq. (1), for the solid phase: the binary interaction parameters ($k_{ij}$) of the three mixtures have been regressed against selected literature data of SLE, SVE, and SLVE. All the data considered in this work are gathered in

Table 1, whereas Table 2 presents all the parameters within Eq. 1 and the $k_{ij}$ of the PR EoS for the three mixtures.

**Table 1.** Literature SLVE, SLE, and SVE data considered in this work.

| Ref. | Kind of data | N° of points | T range [K] | P range [K] | $x_2$ range | $y_2$ range [mol/mol] |
|---|---|---|---|---|---|---|
| (1)$H_2$ + (2)$N_2$ mixture[1] | | | | | | |
| [20] | SVE | 47 | 33 – 62 | 0.13 – 2.53 | | $2\times10^{-6}$ – 0.06 |
| [20] | SLE | 8 | 28 – 32 | 0.51 – 2.53 | 0.6 – 12 | |
| [21] | SLE | 16 | 20 – 32 | 1.26 – 2.53 | 2 – 85 | |
| (1)$N_2$ + (2)$CO_2$ mixture[1] | | | | | | |
| [24] | SVE | 64 | 140 – 190 | 0.51 – 10.1 | | $2\times10^{-4}$ – 0.79 |
| [25] | SLE | 27 | 78 – 115 | 4.05 – 9.12 | 1.6 – 214 | |
| (1)$CH_4$ + (2)$CO_2$ mixture[2] | | | | | | |
| [26] | SLVE | 48 | 97 – 222 | 0.03 – 4.87 | $2\times10^{-3}$ – 0.20 | $1\times10^{-3}$ – 0.12 |
| [27] | SLVE | 21 | 194 – 216 | 0.92 – 4.86 | | |
| [28] | SLVE | 10 | 165 – 210 | 1.90 – 4.85 | 0.18 – 0.74 | $6\times10^{-3}$ – 0.18 |
| [29] | SLVE | 9 | 112 – 170 | 0.09 – 2.31 | $2\times10^{-4}$ – 0.03 | |
| [30] | SLVE | 6 | 166 – 200 | 1.95 – 4.98 | 0.02 – 0.05 | |

[1] $x_2$ range given in ppm
[2] $x_2$ range given in mol/mol

Authors stress that the objective of this section is not proposing a particular and optimal set of binary interaction parameters for the three mixtures, the aim is merely validating the model by showing the good agreement between selected data and modeling results in order to provide reliability to the whole qualitative analysis of modeling results presented in this section. As a consequence, $k_{ij}$ have not been regressed as usual by minimizing an objective function based on the difference between experimental and calculated data, rather their values have been fixed by observing the agreement between data and modelling results in graphs and figures.

**Table 2:** Parameters within the classical approach, Eq. (1), and binary interaction parameters of the PR EoS.

| $\Delta H_{m,2}$ [kJ/mol] | $T_{T,2}$ [K] | $\Delta H_{SS,2}$ [kJ/mol] | $T_{SS,2}$ [K] | $k_{ij}$ |
|---|---|---|---|---|
| (1)$H_2$ + (2)$N_2$ mixture | | | | |
| 0.72 | 63.149 | 0.215 | 35.62 | 0 |
| (1)$N_2$ + (2)$CO_2$ mixture | | | | |
| 9.019 | 216.58 | | | $9.7\times10^{-4} \times T - 0.14419$ |
| (1)$CH_4$ + (2)$CO_2$ mixture | | | | |
| 9.019 | 216.58 | | | 0.1 |

For the $H_2$ + $N_2$ system, the solubility of solid nitrogen in vapor and liquid hydrogen given in [20] and [21] have been used as reference (see Table 1), and a null value of $k_{ij}$ appears to be sufficiently consistent for representing these data.

According to Table 2, it should be noted that for the modeling of the SLE, SVE, and SLVE behavior of the $H_2$ + $N_2$ system, both the melting ($T_T$ = 63.149 K and $\Delta H_m$ = 0.72 kJ/mol, [22]) and the solid-solid transition ($T_{SS,i}$ = 35.62 K and $\Delta H_{SS,i}$ = 0.215 kJ/mol, [23]) properties of nitrogen have been used in the classical approach, Eq. (1).

The qualitative comparison between experimental values and modeling results is illustrated in Fig. 7. Fig. 7 shows the evolution of the solubility of solid nitrogen in hydrogen with temperature: literature data are represented by red symbols; continuous lines refer to modeling results; horizontal dashed lines are representative of SLVE conditions. Data and modeling results deal with the SVE and SLE behavior of the system at 0.1 MPa, 0.5 MPa, 1 MPa, 1.3 MPa, 1.5 MPa, and 2.5 MPa.

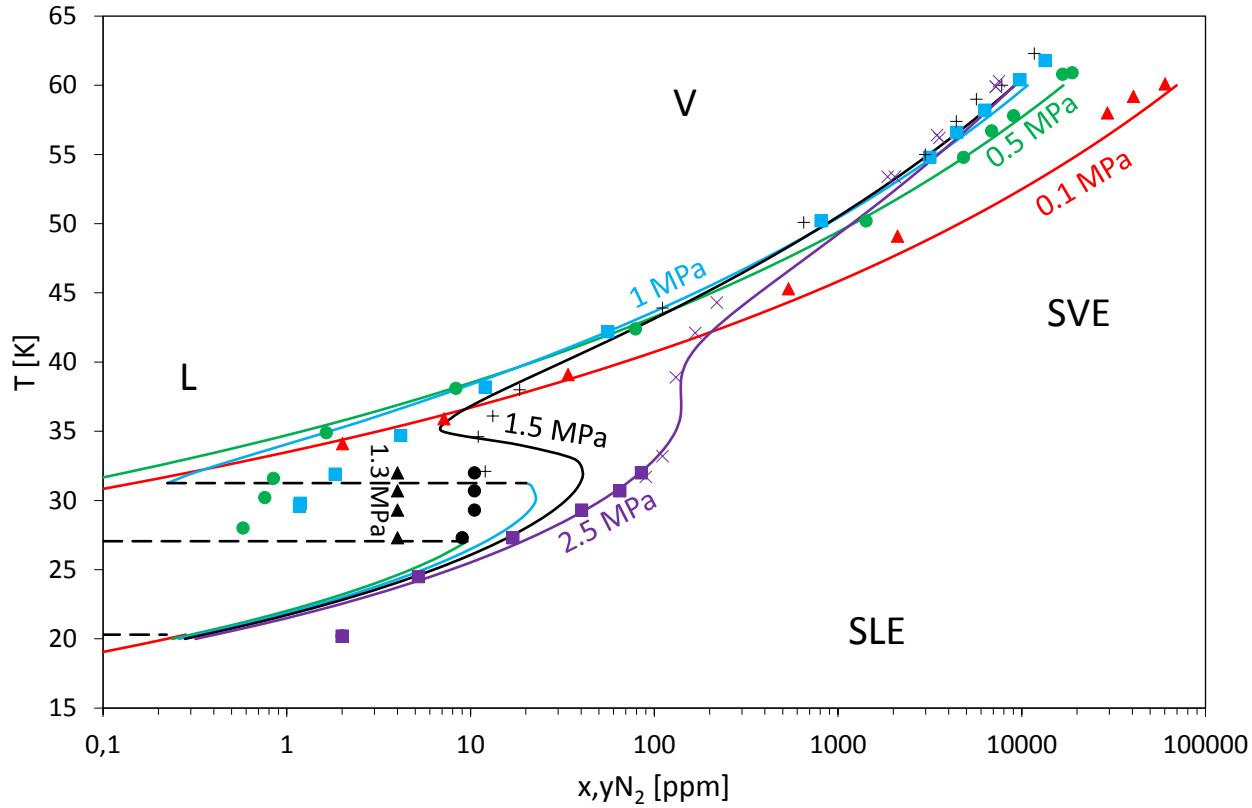


**Fig. 7.** Solubility of solid nitrogen in hydrogen.
L : liquid phase: V : vapor phase; SLE : solid-liquid equilibrium; SVE: solid-vapor equilibrium.
Literature values: ▲, ●, ■, +, ×: Ref. [20]; ▲, ●, ■ : Ref. [21]. Calculated values: — : SLE and SVE; – – : SLVE temperature.

Given the good qualitative agreement between data and modeling results, the model has been applied for calculating the solubility limits of solid nitrogen in vapor and liquid hydrogen in the temperature and pressure range of 20 K ≤ T ≤ 60 K (step of 1 K) and 0.1 MPa ≤ P ≤ 3 MPa (step of 0.1 MPa). The results are illustrated in the colormap of Fig. 8.

In Fig. 8, the black line is the saturation line of hydrogen; the color bar indicated the key to colors which are associated to a particular value of the logarithm of the solubility of solid nitrogen (in ppm) in the liquid (x) or in the vapor (y) phase.

Close to the saturation line of hydrogen in the low-pressure region, the solubility of nitrogen in the vapor phase at SVE decreases down to about 0.1 ppb (ln $yN_2$ = about -16); at 60 K, the minimum and maximum solubilities of nitrogen in hydrogen are about 0.9% and 7%, respectively. At 20 K (value close to the normal boiling point of hydrogen), the solubility of nitrogen is about 0.1 ppb in the vapor phase and 0.2 ppm in the liquid phase. From Fig. 8 it is possible to state that the solubility

of solid nitrogen always decreases for decreasing temperatures at a given pressure only in the high-pressure region (P > 2.5 MPa), whereas it increases at lower pressures (in the 1.3 MPa < P < 2.5 MPa range) when crossing the critical-point region of hydrogen before decreasing again at low temperatures.

This last behavior is related to the S-loop shape of the solubility of nitrogen in hydrogen, (qualitatively shown in Fig. 6), and it precedes the discontinuous behavior encountered at lower pressures (P < critical pressure of hydrogen) due to the existence of SVE and SLE conditions separated by a SLVE temperature (as in Fig. 3).

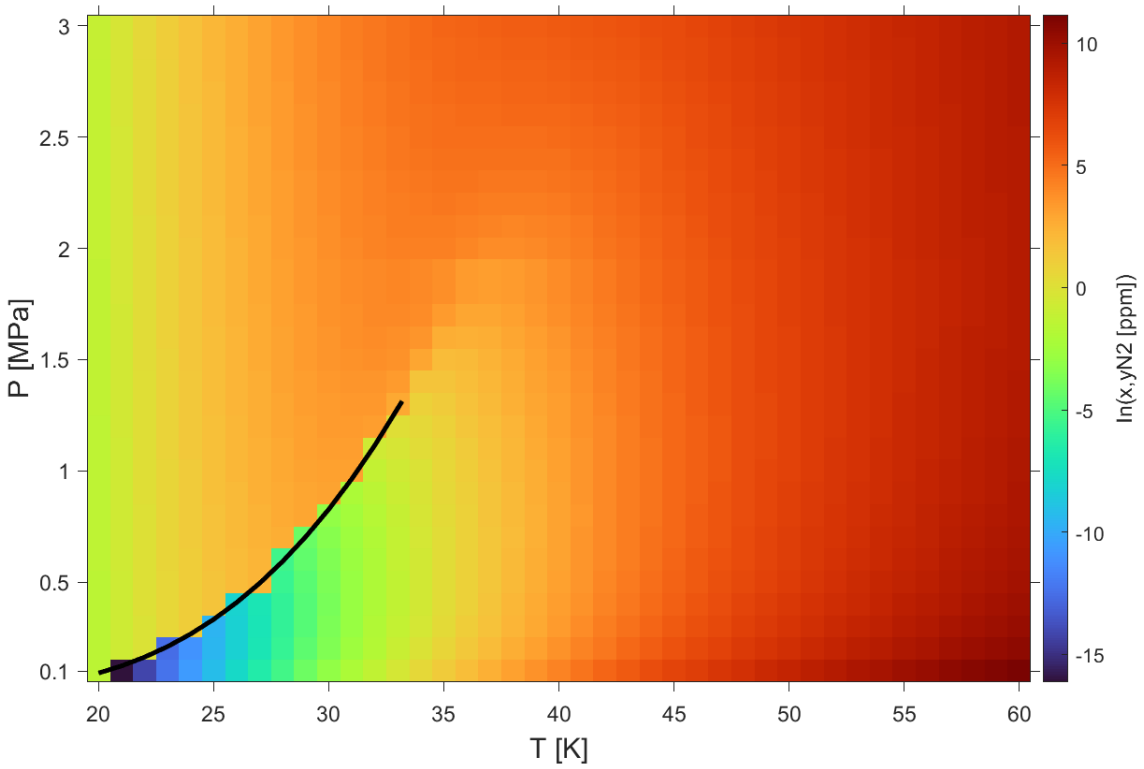


**Fig. 8.** Colormap illustrating the evolution of the calculated solubility of solid nitrogen in hydrogen in the pressure-temperature diagram.
**—** : VLE of hydrogen.

At a given pressure P, the solubility of solid nitrogen in hydrogen at a given temperature T can be compared with the solubility at the warmer temperatures $T^+$ ($T < T^+ \leq 60$ K). When the solubility at P and T is lower than the solubility at all the temperature within the $T^+$-range, the liquefaction (or

cooling) process down to T does not present any risk of crystallization if the purification unit reduces the nitrogen-content in the feed down to (or slightly below) the solubility limit of nitrogen in hydrogen at P and T. This happens for instance at 3 MPa in Fig. 8; at given temperature, the solubility is lower than those at all the preceding temperatures and the color associated to the logarithm of the solubility passes monotonically from about 10 (dark red) to about -5 (green).

To the contrary, if the solubility at T (and given pressure) is higher than that at some $T^+$ warmer temperatures, the purification is not suitable and freeze-out conditions could be thermodynamically encountered at temperatures higher than T if the purification unit reduces the nitrogen-content in the feed only down to (or slightly below) the solubility limit of nitrogen in hydrogen at P and T rather than at P and $T^+$.

This happens for instance in the sub-critical region (with respect to hydrogen) and also at pressures up to about 2.5 MPa. For instance, at 1.5 MPa the solubility at 30 K (approaching $\ln xN_2 = 5$) is higher than that at 35 K (approaching $\ln xN_2 = 0$), as shown by the color which is almost the same (orange) at 30 K and 40 K but is yellow in between (lower solubility).

This behavior can also be resumed as in Fig. 9. Considering a cryogenic (cooling or liquefaction) process at a given pressure P, each $H_2 + N_2$ mixture leaving the cryogenic facility at a temperature T in the white area of the pressure-temperature diagram of Fig. 9 is in the fluid phase if the purification unit lowered the nitrogen-content in the feed down to the solubility limit of nitrogen in hydrogen at same P and T. In other words, a suitable purification is applied for avoiding solid deposition.

To the contrary, nitrogen can solidify at the given pressure P from a thermodynamic point of view for those temperatures pointed out by a color different from white if the purification unit has been tailored for reducing the nitrogen-content down to its solubility at P and T rather than at P and the temperature (higher with respect to T) where the minimum of solubility occurs (see Figs. 3 and 6).

The color bar in Fig. 9 indicates indeed the difference between the temperature reached by the $H_2 + N_2$ mixture thanks to the cryogenic process at a given pressure and the temperature at which the

minimum of solubility occurs; for instance, if the nitrogen-content in a $H_2$ + $N_2$ mixture is decreased according to the solubility of nitrogen in liquid hydrogen at 21 K and 1 MPa, the crystallization risk is not negligeable because the supposed sufficiently purified mixture will encounter the SVE region (as in Fig. 3) at a temperature that is 11 degrees higher than the final liquefaction one (neglecting the last expansion step down to atmospheric pressure).

It is possible to appreciate in Fig. 9 the effect of the S-loop shape of the solubility (Fig. 6) on the extension of the region affected by such a behavior with respect to the position of the saturation line of hydrogen.

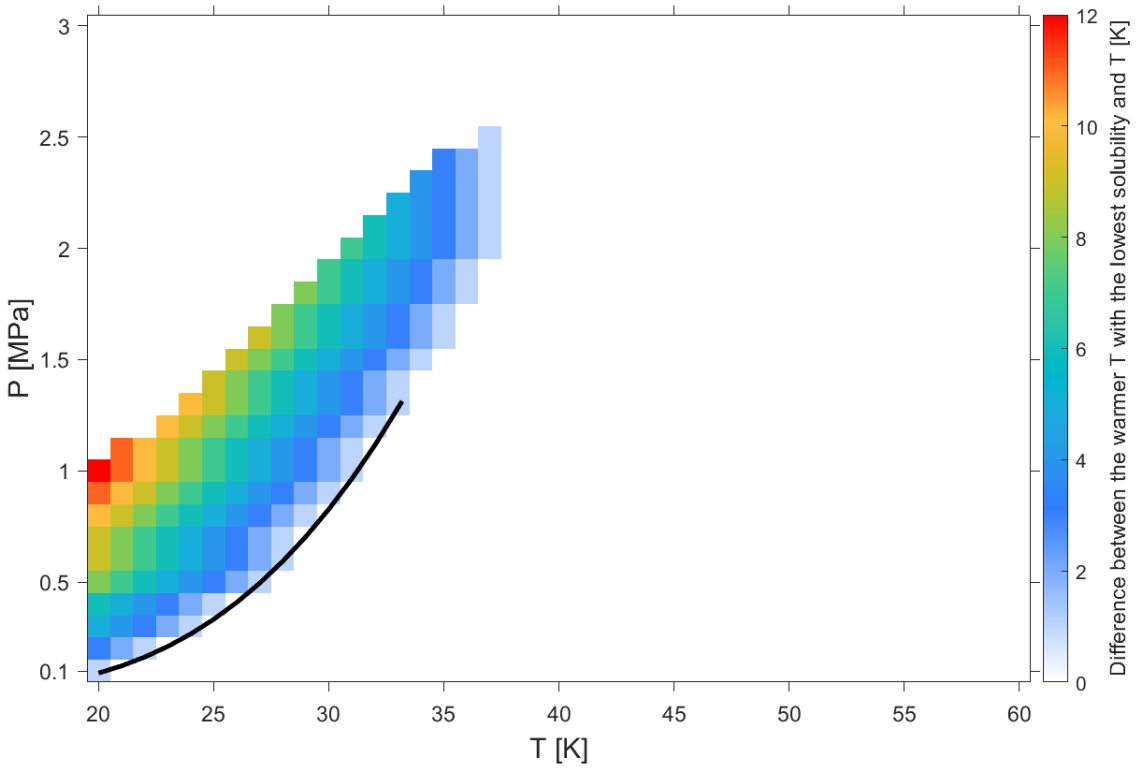


**Fig. 9.** Colormap illustrating the difference between the temperature $T^+$ characterized by the lowest solubility of nitrogen in hydrogen at given pressure and a given temperature T ($T < T^+$).
**—** : VLE of hydrogen.

Similar analysis and graphs are presented in the following for the $N_2$ + $CO_2$ and $CH_4$ + $CO_2$ systems.

For the former mixture, the SVE data of [24] and SLE data of [25] given in Table 1 have been used for "regressing" a temperature-dependent function for the binary interaction parameter of the PR EoS ($k_{ij}$ = 0.00097 × T – 0.14419) when it is coupled with the classical approach for carbon dioxide ($T_T$ = 216.58 K and $\Delta H_m$ = 9.019 kJ/mol, [22]), Eq. (1), values given in Table 2.

The experimental SVE and SLE data are compared to modeling results in Fig. 10 and 11, respectively.

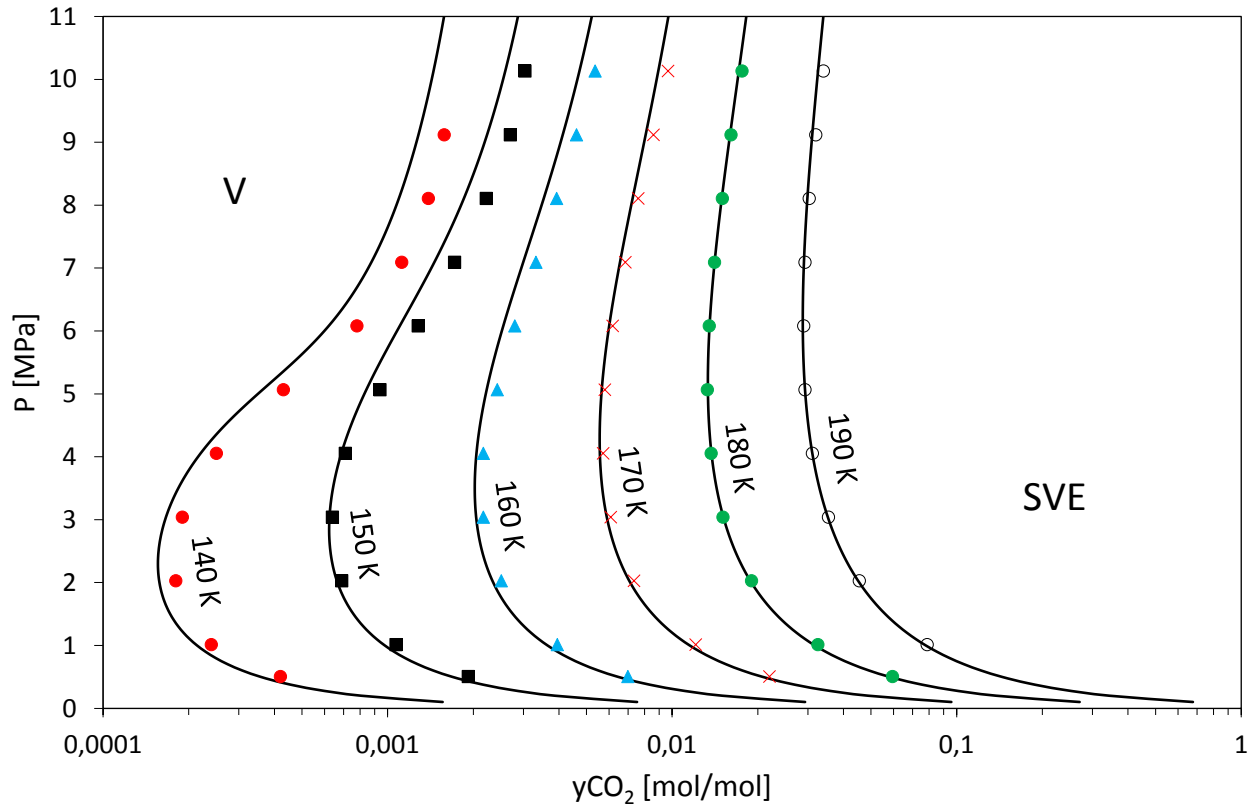


**Fig. 10.** Solubility of solid carbon dioxide in vapor nitrogen.
V : vapor phase: SVE : solid-vapor equilibrium. Symbols: literature values from Ref. [24]. Calculated values: —.

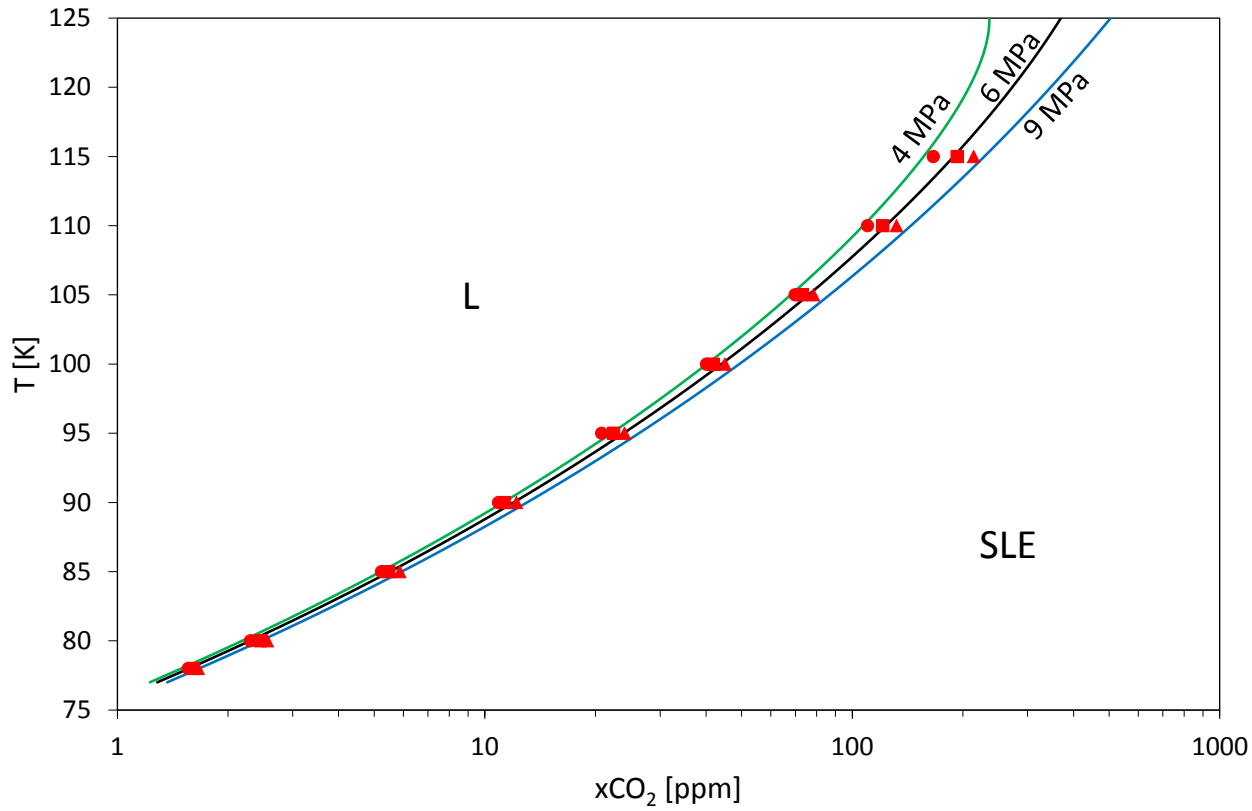


**Fig. 11.** Solubility of solid carbon dioxide in liquid nitrogen.
L : liquid phase: SLE : solid-liquid equilibrium. Symbols: literature values from Ref. [25]. Calculated values: —.

Given the satisfactory agreement between data and modeling results, the model has been applied for calculating the solubility limits of solid carbon dioxide in vapor and liquid nitrogen in the temperature and pressure range of 77 K ≤ T ≤ 190 K (step of 1 K) and 0.1 MPa ≤ P ≤ 10 MPa (step of 0.1 MPa). The results are illustrated in the colormap of Fig. 12, where the black line is the saturation line of nitrogen; the color bar indicated the key to colors which are associated to a particular value of the logarithm of the solubility of solid carbon dioxide (in ppm) in the liquid (x) or in the vapor (y) phase.

Being the $N_2 + CO_2$ system of the same kind of the $H_2 + N_2$ system (type IIIc), the analysis done for Fig. 8 is valid also for Fig. 12.

Solid carbon dioxide is, on average, more soluble in nitrogen than solid nitrogen in hydrogen: the lowest calculated solubility of carbon dioxide in nitrogen is about 4 ppm (at 0.1 MPa and 78 K, ln $xCO_2$ = -12.4), whereas the lowest calculated solubility of nitrogen in hydrogen is about 0.01 ppm

(at 0.1 MPa and 21 K, ln $xN_2$ = -16.1). At 190 K (maximum temperature investigated in this work), the minimum and maximum solubilities of carbon dioxide in nitrogen are about 3% and 68%, respectively.

From Fig. 12 it is possible to state that the solubility of solid carbon dioxide always decreases for decreasing temperatures at a given pressure only in the high-pressure region (P > 6 MPa), whereas it increases at lower pressures (in the 3.5 MPa < P < 6 MPa range) when crossing the critical-point region of nitrogen before decreasing again at low temperatures.

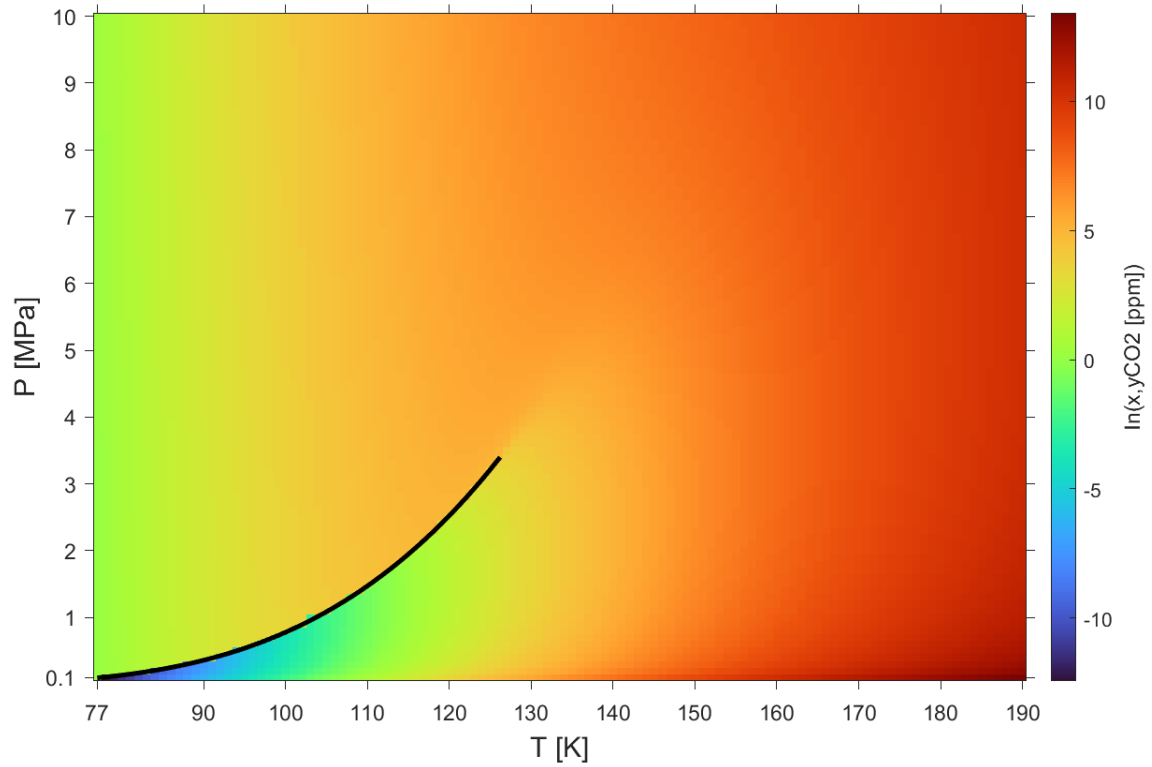


**Fig. 12.** Colormap illustrating the evolution of the calculated solubility of solid carbon dioxide in nitrogen in the pressure-temperature diagram.
**—** : VLE of nitrogen.

Similarly to Fig. 9, the solubility of solid carbon dioxide in nitrogen at a given pressure and temperature T can be compared with the solubility at the same pressure but at warmer temperatures $T^+$ ($T < T^+ \leq 190$ K).

Considering a cryogenic (cooling or liquefaction) process at a given pressure P, if pressure-temperature couple (being this temperature T the temperature of a $N_2$ + $CO_2$ mixture leaving the cryogenic facility) falls in the white area of the pressure-temperature diagram of Fig. 13, then the mixture will be in the fluid phase if the purification unit lowered the nitrogen-content in the feed down to the solubility limit of carbon dioxide in nitrogen at same P and T. In other words, a suitable purification is applied for avoiding solid deposition.

To the contrary, carbon dioxide solidifies at the given pressure P from a thermodynamic point of view for those temperatures pointed out by a color different from white if the purification unit has been tailored for reducing the carbon dioxide-content down to its solubility limit at P and T rather than at P and the temperature (higher with respect to T) where the minimum of solubility occurs.

The color bar in Fig. 13 indicates indeed the difference between the temperature reached by the $N_2$ + $CO_2$ mixture thanks to the cryogenic process at a given pressure and the temperature at which the minimum of solubility occurs; for instance, if the carbon dioxide-content in a $N_2$ + $CO_2$ mixture is decreased according to the solubility of carbon dioxide in liquid nitrogen at 77 K and 1 MPa, the crystallization risk is not negligeable because the supposed sufficiently purified mixture will encounter the SVE region (as in Fig. 3) at a temperature that is 26 degrees higher than the final liquefaction one (neglecting the last expansion step down to atmospheric pressure).

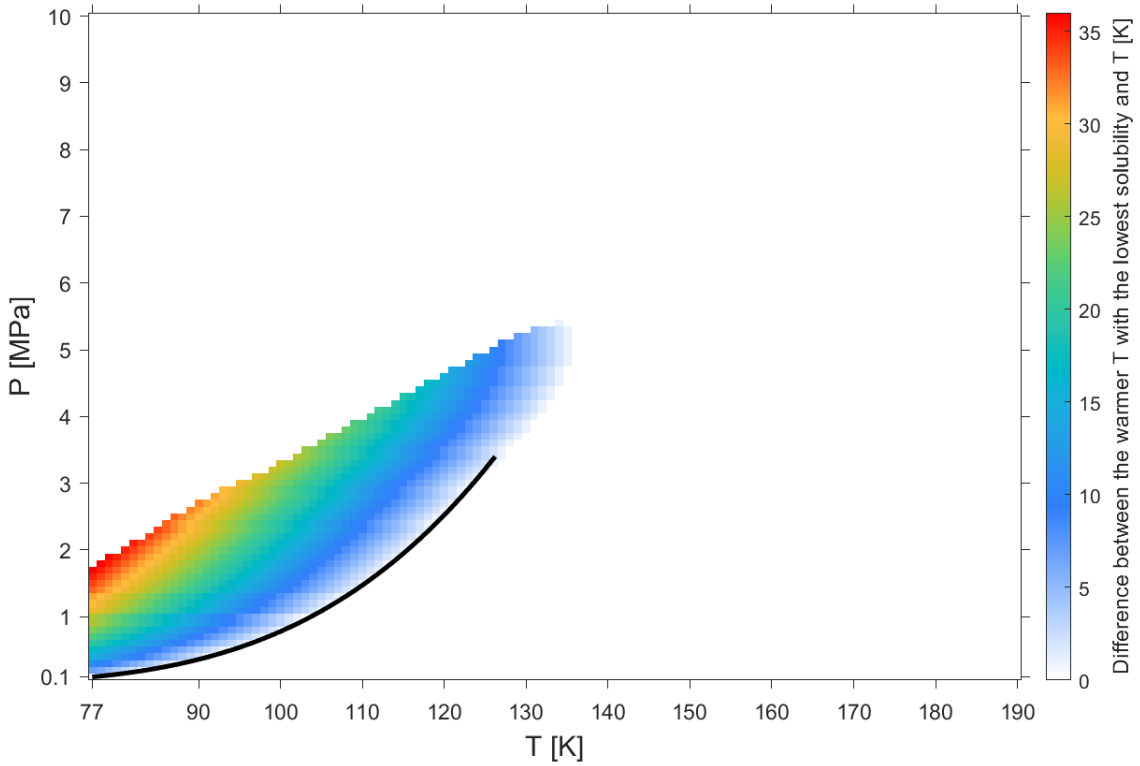


**Fig. 13.** Colormap illustrating the difference between the temperature $T^+$ characterized by the lowest solubility of carbon dioxide in nitrogen at given pressure and a given temperature T ($T < T^+$). ▬ : VLE of nitrogen.

For the $CH_4$ + $CO_2$ system, the SLVE data of [26-30] gathered in Table 1 have been selected in this work as reference for evaluating a value of the binary interaction parameter suitable for the PR EoS when coupled with Eq. (1). A value of $k_{ij}$ equal to 0.1 has been found to provide satisfactory results as illustrated in Figs. 14 and 15.

Fig. 14 compares the literature SLVE pressures and temperatures (symbols) to the calculated SLVE locus (black line) leaving the triple point of carbon dioxide; the magenta lines are the sublimation, melting and saturation lines of carbon dioxide.

Fig. 15 compares the literature solubilities of carbon dioxide in the vapor and liquid phases at SLVE (symbols) to the calculated SLVE compositions in the liquid (black line) and vapor (red line) phases originating at the triple-point temperature of carbon dioxide.

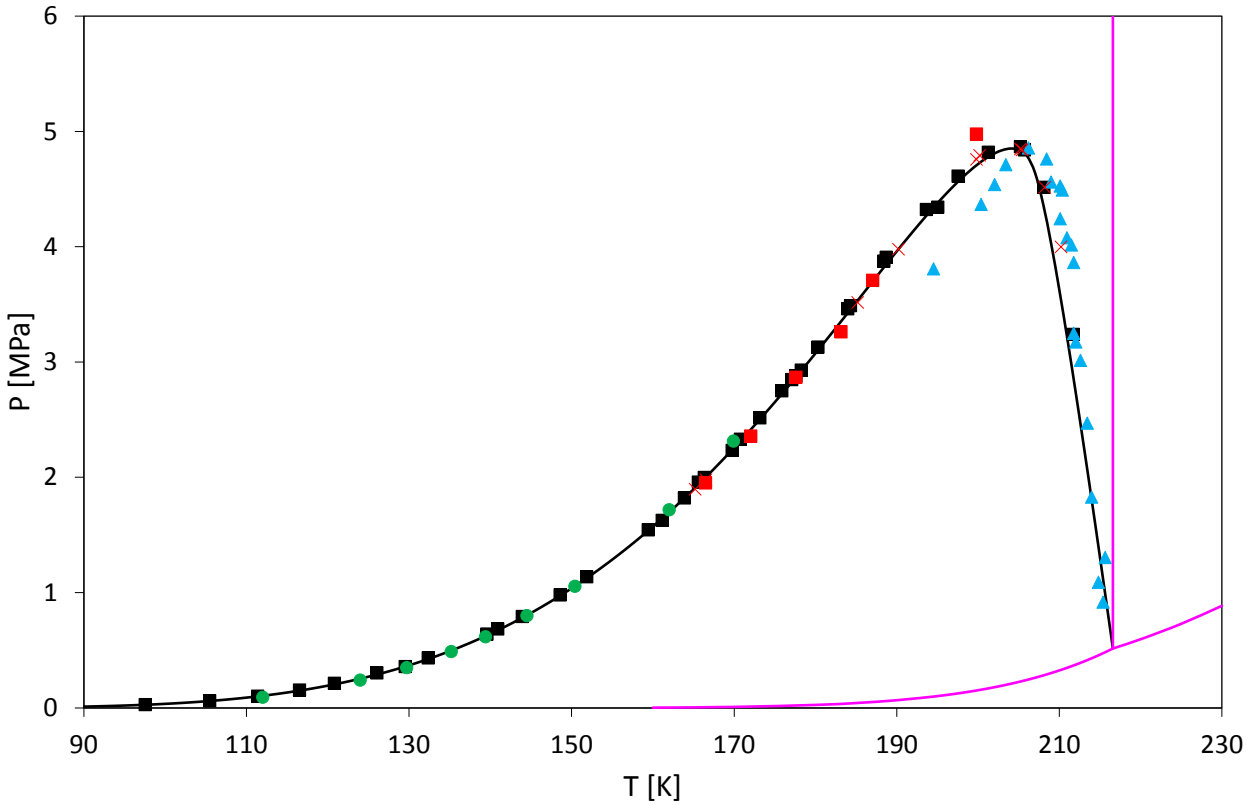


**Fig. 14.** SLVE locus of the methane + carbon dioxide system.
Literature values: ■ : [26]; ▲ : [27]; × : [28]; ● : [29]; ■ : [30]. Calculated values: — : SLVE; : — : SVE, VLE, and SLE of carbon dioxide.

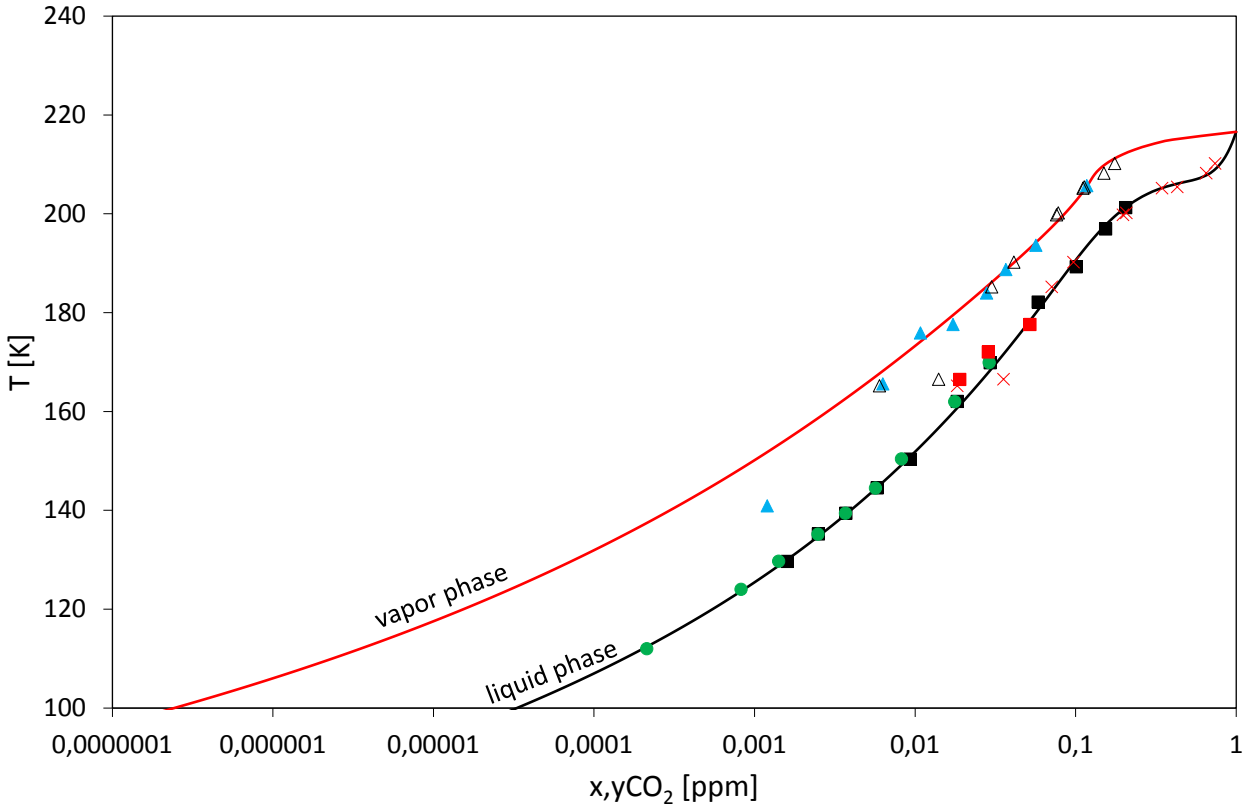


**Fig. 15.** Solubilities of carbon dioxide in liquid and vapor phases at SLVE for the methane + carbon dioxide system.
Literature values : ■ : $xCO_2$ [26]; ▲ : $yCO_2$ [26]; × : $xCO_2$ [28]; Δ : $yCO_2$ [28]; ● : $xCO_2$ [29]; ■ : $xCO_2$ [30]. Calculated SLVE lines: — : vapor phase; — : liquid phase.

Given the good qualitative agreement between data and modeling results, the model has been applied for calculating the solubility limits of solid carbon dioxide in vapor and liquid methane in the temperature and pressure range of 111 K ≤ T ≤ 216.58 K (step of 1 K) and 0.1 MPa ≤ P ≤ 10 MPa (step of 0.1 MPa). The results are illustrated in the colormap of Fig. 16.

In Fig. 16, the black line is the calculated SLVE locus, whereas the magenta lines are the SVE and SLE conditions of carbon dioxide; the color bar indicated the key to colors which are associated to a particular value of the logarithm of the solubility of solid carbon dioxide (in ppm) in the liquid (x) or in the vapor (y) phase.

At given pressure P1, the solubility of carbon dioxide in methane always monotonically decreases for decreasing temperatures in the considered temperature range provided that P1 is higher than the maximum pressure of the SLVE locus (calculated value = 4.85 MPa at about 204 K).

At a pressure P2 lower than 4.85 MPa but higher than the triple-point pressure of carbon dioxide (about 0.52 MPa), two SLVE conditions occur: one (at temperature T1) in the high-temperature region (T > 204 K) and one (at temperature T2) in the low-temperature region (T < 204 K). At P2, the solubility of carbon dioxide (i) decreases in the liquid phase from 100% on the melting line of carbon dioxide down to T1 (high-temperature SLVE), (ii) decreases in the vapor phase from T1 down to T2, and (iii) decreases in the liquid phase from T2 (low-temperature SLVE) down to 111 K.

At pressure P3 lower than the triple-point pressure of carbon dioxide, only the low-temperature SLVE condition occurs at a temperature T2. At P3, the solubility of carbon dioxide (i) decreases in the vapor phase from 100% on the sublimation line of carbon dioxide down to T2 (low-temperature SLVE), and (ii) decreases in the liquid phase from T2 down to 111 K:

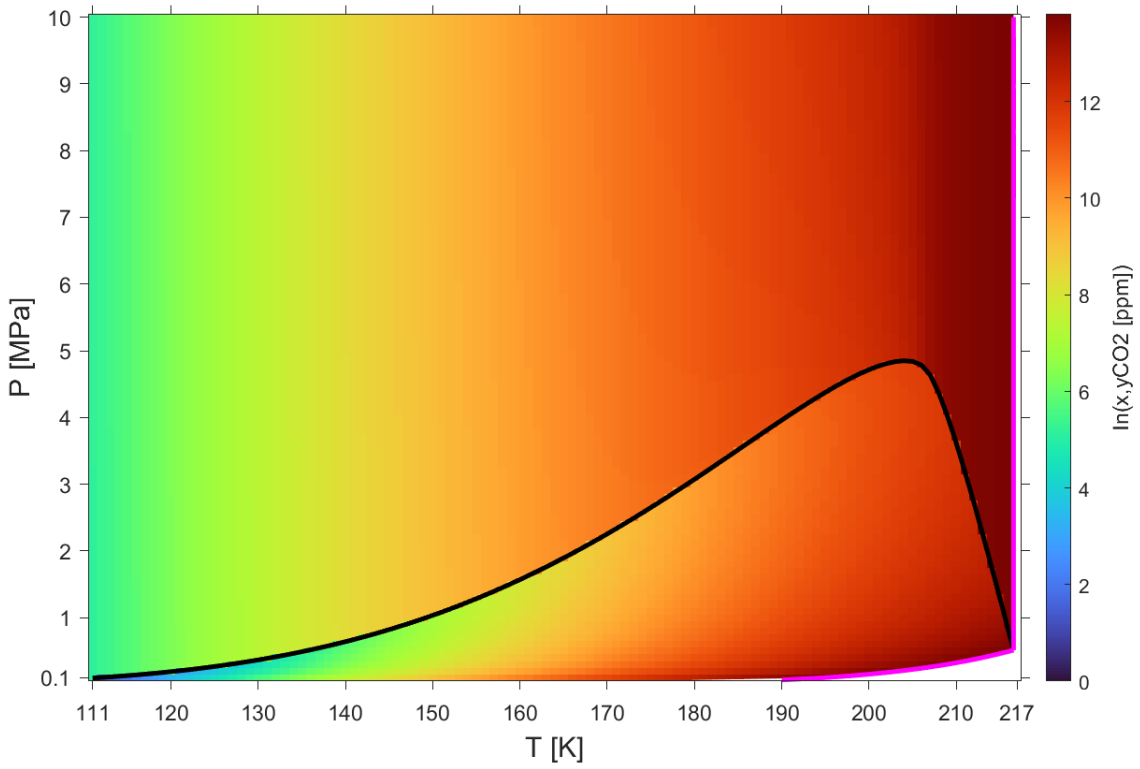


**Fig. 16.** Colormap illustrating the evolution of the calculated solubility of solid carbon dioxide in methane in the pressure-temperature diagram.
Calculated values: ▬ : SLVE of the mixture; ▬ : SVE and SLE of carbon dioxide.

In the pressure range 0.52 MPa < P2 < 4.58 MPa, the SLVE conditions of the system are such that at both T1 and T2 the solubility of carbon dioxide in the vapor phase is lower than the solubility in the liquid phase, and this happens also at the unique SLVE temperature T2 encountered at a pressure P3 lower than the triple-point pressure of carbon dioxide. As a consequence, if the carbon dioxide-content in a $CH_4$ + $CO_2$ system is decreased in the purification unit according to the solubility limit of carbon dioxide in the liquid phase at pressures P2 or P3 and temperature T < T2, crystallization could occur at higher temperatures, as illustrated in Fig. 17.

As an example, a $CH_4$ + $CO_2$ mixture purified down to 1050 ppm of carbon dioxide to respect the solubility limit of carbon dioxide in the liquid phase at 1 MPa and 126 K (calculated value = 1064 ppm) presents a risk of crystallization seeing that the solubility of carbon dioxide in the vapor phase is 1006 ppm at 150 K, namely at a temperature 25 degrees higher than the final liquefaction temperature.

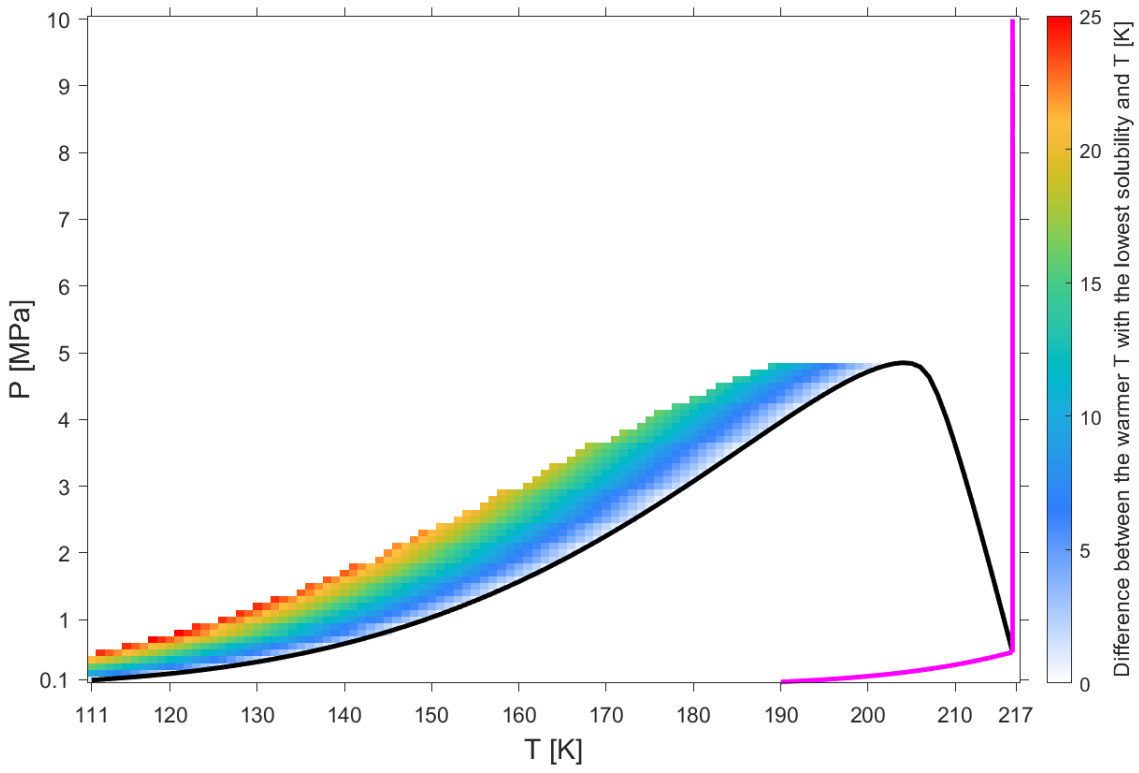


**Fig. 17.** Colormap illustrating the difference between the temperature $T^+$ characterized by the lowest solubility of carbon dioxide in methane at given pressure and a given temperature T (T < $T^+$).

Calculated values: ▬ : SLVE of the mixture; ▬ : SVE and SLE of carbon dioxide.

## 5 Conclusions

In dealing with the design of cryogenic processes (among which liquefaction) applied to gaseous mixture (rich for instance in hydrogen, methane, main air components, and carbon dioxide), efforts are in place to avoid the risks of crystallization of solid formers while decreasing the temperature of the mixture.

Two variables are known to have an impact on the evolution of the solubility of a solid former in the solvent of a binary mixture, i.e., the system temperature (solubility decreases for decreasing temperatures) and the density of the solvent (solubility decreases for decreasing density).

As portrayed in the phase equilibrium behavior of Fig. 3 (valid not only for type I, IIIa, and IIIc mixtures, but also types II, IV-VI are concerned since Fig. 2(A) should be also valid for their low-temperature phase equilibrium behavior), the first line involving a solid phase that is encountered in the liquefaction process is the one representing the composition of the vapor phase at solid-vapor equilibrium when the liquefaction pressure is lower than the critical-point pressure of the gas to be liquefied. This vapor can be either at SVE or VLE, the underlying difference is the composition of the light component (LC) in the gaseous mixture leaving the purification unit and feeding the liquefaction unit.

In case of having a LC-content lower than the composition of the vapor phase at the SLVE at the pressure of the unit, the first risk of solidification of the impurity is related to the deposition process from a vapor phase rather than a solidification from a liquid phase at lower temperatures.

As illustrated in the phase equilibrium behavior of Fig. 6 (valid for type IIIa and IIIc mixtures), the first line that is encountered in the liquefaction process could still be the one representing the composition of the vapor phase even if the liquefaction pressure is higher than the critical-point pressure of the gas to be liquefied because of the effect of the solvent density on the solubility.

In both cases (Figs. 3 and 6), safe allowances for the solubility limits of impurities in binary mixtures with light gases appear then related to the proper description not only of the SLE at low temperatures, but also of the phase equilibrium behavior close to the SLVE temperature and the saturation temperature of pure LC at the pressure of the process.

In dealing with the crystallization risks, the constraint should be then the evolution of the composition of the solid former in the vapor phase along the vapor branch of the SVE down to the SLVE temperature (Fig. 3) or the S-loop shape temperature range (Fig. 6), which could be more restrictive (according to the liquefaction pressure) then the composition of the solid former in the liquid phase at the SLE occurring at lower temperatures.

To conclude, authors want to stress that the discussion here presented is only based on thermodynamic aspects of solid-fluid equilibria and lacks then information concerning kinetics and non-equilibrium phenomena involved in the liquefaction/cooling process.

## CRediT authorship contribution statement

Marco Campestrini: Conceptualization, Methodology, Software, Investigation, Writing - Original Draft. Paolo Stringari: Conceptualization, Methodology, Validation, Writing - Review & Editing, Supervision; Salem Hoceini: Conceptualization, Methodology, Validation, Investigation, Writing - Review & Editing. Nicolò Baiguini: Software, Data Curation, Resources, Investigation, Writing - Review & Editing.

## Declaration of competing interest

On behalf of all the authors, the corresponding author declare that they have no known competing financial interests or personal relationships with other people or organizations that could have appeared to influence the work reported in this paper.

## References

[1] Smith EM. Liquid oxygen for aerospace applications. Int. J. Hydrog. Energy 14 (1989) 831–837. doi.org/10.1016/0360-3199(89)90020-7

[2] Gorbatskii YV, Gerasimov VE, Peredel'skii VA, Darbinyan RV, Lyapin AI, Izotov NI. Use of LNG cryogenic technology during refining of associated petroleum gases. Chem. Pet. Eng. 40 (2004) 521–527. doi.org/10.1007/s10556-005-0003-z

[3] Su C-L, Lee C-N, Chen H-C, Feng L-P, Lin H-W, Chiang L-L. Comparison of domiciliary oxygen using liquid oxygen and concentrator in northern Taiwan. J. Formos. Med. Assoc. 113 (2014), 23–32. doi.org/10.1016/j.jfma.2012.03.013

[4] Rada M, Shooshtari A, Ohadi MM. Experimental and numeral simulation of meso-pumping of liquid nitrogen - Application to cryogenic spot cooling of sensors and detectors. Sens. Actuators A Phys. 148 (2008) 271–279. doi.org/10.1016/j.sna.2008.08.008

[5] Nezafati M, Sohn I, Ferguson JB, Park J-S , Cho K, Kim C-S. DFT study on the adsorption and absorption behaviors of liquid nitrogen in the Mg nano alloys synthesized from powder metallurgy. Comput. Mater. Sci. 105 (2015) 18–26. doi.org/10.1016/j.commatsci.2015.04.017

[6] Yatsenko EA, Goltsman BM, Novikov YV, Izvarin AI, Rusakevich IV. Review of modern ways of insulation of reservoirs for liquid hydrogen storage. Int. J. Hydrog. Energy 47 (2022) 41046–41054. doi.org/10.1016/j.ijhydene.2022.09.211

[7] Yin Y, Lam JSL. Bottlenecks of LNG supply chain in energy transition: a case study of China using system dynamic simulation. Energy 250 (2022) 123803. doi.org/10.1016/j.energy.2022.123803

[8] Prausnitz JP, Lichtenthaler RN, de Azevedo EG. Molecular thermodynamics of fluid-phase equilibria, second ed., Prentice-Hall, Englewood Cliffs, NJ, 1986.

[9] Campestrini M. Thermodynamic study of solid-liquid-vapor equilibrium: application to cryogenics and air separation unit. PhD Thesis, MINES ParisTech, Paris, 2014.

[10] Campestrini M, Stringari P. Solubilities of solid n-alkanes in methane: data analysis and models assessment. AIChE J. 64 (2018) 2219–2239. doi.org/10.1002/aic.16071

[11] Langé S, Campestrini M, Stringari P. Phase behavior of system methane + hydrogen sulfide. AIChE J. 62 (2016) 4090–4108. doi.org/10.1002/aic.15311

[12] Stringari P, Campestrini M, Coquelet C, Arpentinier P. An equation of state for solid–liquid–vapor equilibrium applied to gas processing and natural gas liquefaction. Fluid Phase Equilib. 362 (2014) 258−267. doi.org/10.1016/j.fluid.2013.10.020

[13] Baker CJ. Phase equilibrium measurements and advanced modelling for optimising liquefied natural gas production. PhD Thesis, University of Western Australia, 2018.

[14] Kohn JP, Luks KD. Solubility of hydrocarbons in cryogenic LNG and NGL mixtures. Gas Processor Association Research Report 22, 1976.

[15] Teja AS, Smith VS, Sun T, Mendez-Santiago J. Solids deposition in natural gas systems. Gas Processor Association Research Report 171, 2000.

[16] Hottovy JD, Luks KD, Kohn JP. Three-phase liquid-liquid vapor equilibria behavior of certain binary CO2–n-paraffin systems. J. Chem. Eng. Data 26 (1981) 256-258. doi.org/10.1021/je00025a009

[17] van Konynenburg PH, Scott RL. Critical lines and phase equilibria in binary van der Waals mixtures. Phil. Trans. R. Soc. Lond. 298 (1980) 495–540. doi.org/10.1098/rsta.1980.0266

[18] Stringari P, Campestrini M, Gerek Ince N, Bluck D, Hirohama S, Garcia F, Bartuel JJ. Toward an optimized design of the LNG production process: Measurement and modeling of the solubility limits of p-xylene in methane and methane + ethane mixtures at low temperature. Fluid Phase Equilibr. 55 (2022) 113406. doi.org/10.1016/j.fluid.2022.113406

[19] Peng DY, Robinson DB. The characterization of the heptanes and heavier fractions for the GPA Peng-Robinson programs. Gas Processor Association Research Report 28, 1978.

[20] Dokoupil Z, van Soest G, Swenker DPM. On the equilibrium between the solid phase and the gas phase of the systems H2-N2, H2-CO, and H2-N2-CO. Appl. Sci. Res. Sec. A. 5 (1955) 182–240. doi.org/10.1007/BF03184616

[21] Petit P. Solubility of nitrogen in hydrogen below the critical temperature of hydrogen. Compt. Rend. 246 (1958) 1171–1172

[22] Simulis® Thermodynamics, version 2.0.4, ProSim SA, Lab_ege, France

[23] Lipinski L, Kowal A, Szmyrka-Grzebyk A, Manuszkiewicz H, Steur PPM, Pavese F. The α-β transition of nitrogen. Int. J. Thermophys 28 (2007) 1904–1912. doi.org/10.1007/s10765-007-0267-y

[24] Sonntag RE, van Wylen GJ. The solid-vapor equilibrium of carbon dioxide-nitrogen, Adv. Cryog. Eng. 7 (1962) 99–105. doi.org/10.1007/978-1-4757-0531-7_12

[25] Yakimenko NP, Glukh GM, Iomotev MB, Abramova RI. Solubility of carbon dioxide in liquid nitrogen. Russ. J. Phys. Chem. 49 (1975) 116–117.

[26] Davis JA, Rodewald N, Kurata F. Solid-liquid-vapor phase behavior of the methane−carbon dioxide system. AIChE J. 8 (1962) 537−539. doi.org/10.1002/aic.690080423

[27] Donnelly HG, Katz DL. Phase equilibria in the carbon dioxide - methane system. Ind. Eng. Chem. 46 (1954) 511–517. doi.org/10.1021/ie50531a036

[28] Im UK, Kurata F. Phase equilibrium of carbon dioxide and light paraffins in presence of solid carbon dioxide. J. Chem. Eng. Data 16 (1971) 295−299. doi.org/10.1021/je60050a018

[29] Shen T, Gao T, Lin W, Gu A. Determination of CO2 solubility in saturated liquid CH4 + N2 and CH4 + C2H6 mixtures above atmospheric pressure. J. Chem. Eng. Data 57 (2012) 2296–2303. doi.org/10.1021/je3002859

[30] Sterner CJ. Phase Equilibria in the CO2−Methane Systems. Adv. Cryog. Eng. 6 (1960) 467–474. doi.org/10.1007/978-1-4757-0534-8_49